HYDROLOGICAL PROCESSES
Hydrol. Process. **20**, 899–922 (2006)
Published online in Wiley InterScience (www.interscience.wiley.com). DOI: 10.1002/hyp.6120

Point-scale energy and mass balance snowpack simulations in the upper Karasu basin, Turkey

A. Şensoy,[1]* A. A. Şorman,[1] A. E. Tekeli,[2] A. Ü. Şorman[3] and D. C. Garen[4]

[1] *Department of Civil Engineering, Anadolu University, Eskişehir, Turkey*
[2] *Remote Sensing Division, Turkish State Meteorological Services, Ankara, Turkey*
[3] *Department of Civil Engineering, Middle East Technical University, Ankara, Turkey*
[4] *USDA, Natural Resources Conservation Service, National Water and Climate Center, Portland, Oregon, USA*

Abstract:

Since snowmelt runoff is important in the mountainous parts of the world, substantial efforts have been made to develop snowmelt models with many different levels of complexity to simulate the processes at the ground (soil–vegetation), within the snow, and at the interface with the atmosphere. Snow modifies the exchange of energy between the land surface and atmosphere and significantly affects the distribution of heating in the atmosphere by changing the surface albedo and regulating turbulent heat and momentum fluxes at the surface. Thus, for computing the amount of melt, the only strictly correct way is using an energy budget. A two-layer point model (SNOBAL) was applied to calculate the energy and mass balance of snowmelt in the upper Karasu basin, in eastern Turkey, during the 2002–04 snow seasons. The data on snow and climate were provided from automated snow and meteorological stations installed and upgraded to collect high-quality time series data of snow and meteorological variables, such as snow water equivalent, snow depth, precipitation and radiation, with automated data transfer. A number of analyses of snowpack energy and mass balance were carried out to understand the key processes that have major impacts on the snow simulation. Each form of energy transfer was evaluated during snow accumulation and ablation periods using a 2 h computational time step. The model results are appraised with respect both to temporal distribution (the model application for three consecutive snow seasons at one site) and to areal evaluation (the model application to three different sites for one season). The model performance is evaluated by comparing the results with observed snow water equivalent, snow depth and lysimeter yield. Copyright © 2006 John Wiley & Sons, Ltd.

KEY WORDS snow modelling; energy and mass balance; upper Karasu basin; Turkey

INTRODUCTION

For basins in which snow is a significant part of the hydrological cycle, information on timing, magnitude and contributing area of snowmelt is required for successful water and resource management. Eastern Turkey is such an area; however, it is an understudied part of the world in this regard. To develop the information needed to support water management objectives in this area, a combined monitoring and modelling approach is necessary. The overall objective of the study described in this paper is, therefore, to obtain a better understanding of the key processes that have major impacts on snow accumulation and ablation for the eastern part of Turkey. This is accomplished using monitored data from the sites and a model with an accurate representation of the energy and mass balance of the snowpack at a point scale at several sites with small computational time intervals. The specific aims that are addressed include a theoretical understanding of snow processes, testing a process-based snow model capable of simulating accumulation and ablation at a point scale, the calculation of temporal variations in snowmelt and the validation of model results. The data

* Correspondence to: A. Şensoy, Department of Civil Engineering, Anadolu University, Eskişehir, Turkey. E-mail: sensoy@metu.edu.tr

Received 22 June 2005
Accepted 6 October 2005

Copyright © 2006 John Wiley & Sons, Ltd.

on snow and climate are provided from automated snow and meteorological stations installed and upgraded to collect data with automated data transfer. Each form of energy transfer is evaluated during snow accumulation and ablation periods using a 2 h computational time step. The model performance is evaluated by comparing the results with observed snow water equivalent (SWE), snow depth and lysimeter yield.

SITE DESCRIPTION AND IMPORTANCE OF THE STUDY

The Rivers Euphrates and Tigris and their tributaries served as the cradle for many civilizations that developed in Mesopotamia, 'the land between two rivers'. The River Euphrates, the longest in southwest Asia (2700 km), is formed by the union of two major tributaries: the Karasu, which rises in the highlands of eastern Turkey, and the Murat, which originates north of Lake Van (Cullen and Menocal, 2000). The Euphrates basin is largely fed from snow precipitation over the uplands of northern and eastern Turkey. About two-thirds of the precipitation occurs in winter, during which all precipitation falls as snow and which may remain half of the year. This is followed by a sustained period of high flows during the spring resulting from melting of the snowpack. This not only causes extensive spring flooding, inundating large areas, but also the loss of much needed water during the summer season (Altınbilek, 2004).

The Karasu basin, a sub-basin of the River Euphrates, is the test basin for this study (Figure 1). The region is mountainous and, according to the long-term analysis of the hydrographs, snowmelt constitutes 60–70% of total annual streamflow volume (Kaya, 1999). Most of the water that originates from snowmelt contributes to large reservoirs located on the River Euphrates in Turkey. The study area is basically the headwaters, the upper Karasu basin, represented by the drainage area of stream gauging station 2154 (40°45′E, 39°56′N; Figure 2). The basin has an area of 2818 km^2, and the elevation within the basin ranges from 1640 to 3112 m, with a hypsometric mean elevation of 2112 m. The area is predominately steppe (a plain without trees other than those near rivers), which may be semi-desert or covered with grass or shrubs or both, depending on the season; forest cover is only 1·5% of the total basin area.

Although there have been previous applications of snowmelt models in this basin (e.g. Snowmelt Runoff Model (Kaya, 1999; Tekeli, 2005); HBV (Şorman, 2005); HEC-1 (Şensoy *et al.*, 2003)), these are all based on the degree-day approach and cannot be used to evaluate the energy dynamics of snowmelt. With the ultimate

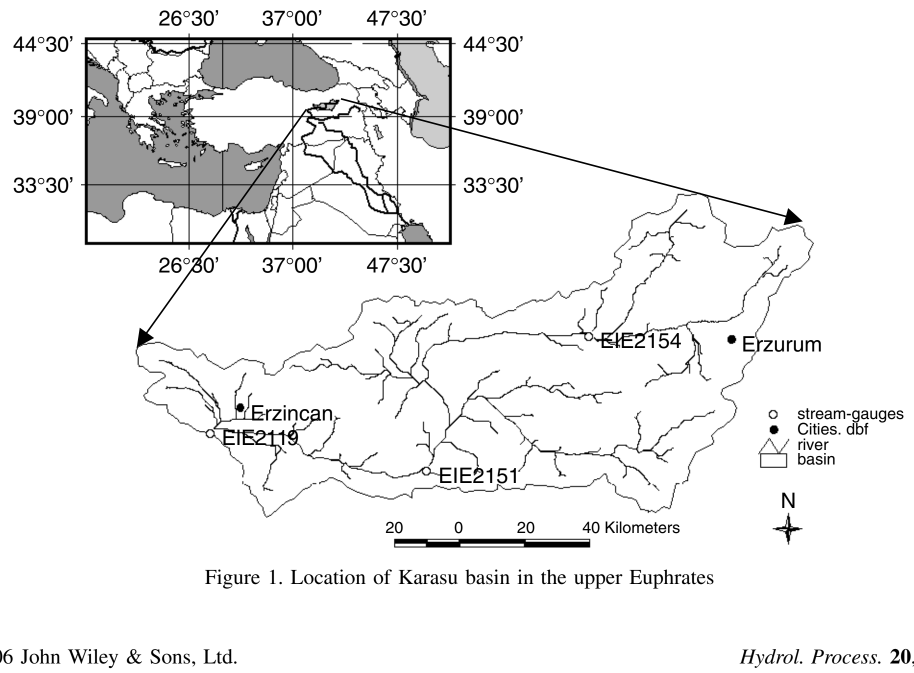

Figure 1. Location of Karasu basin in the upper Euphrates

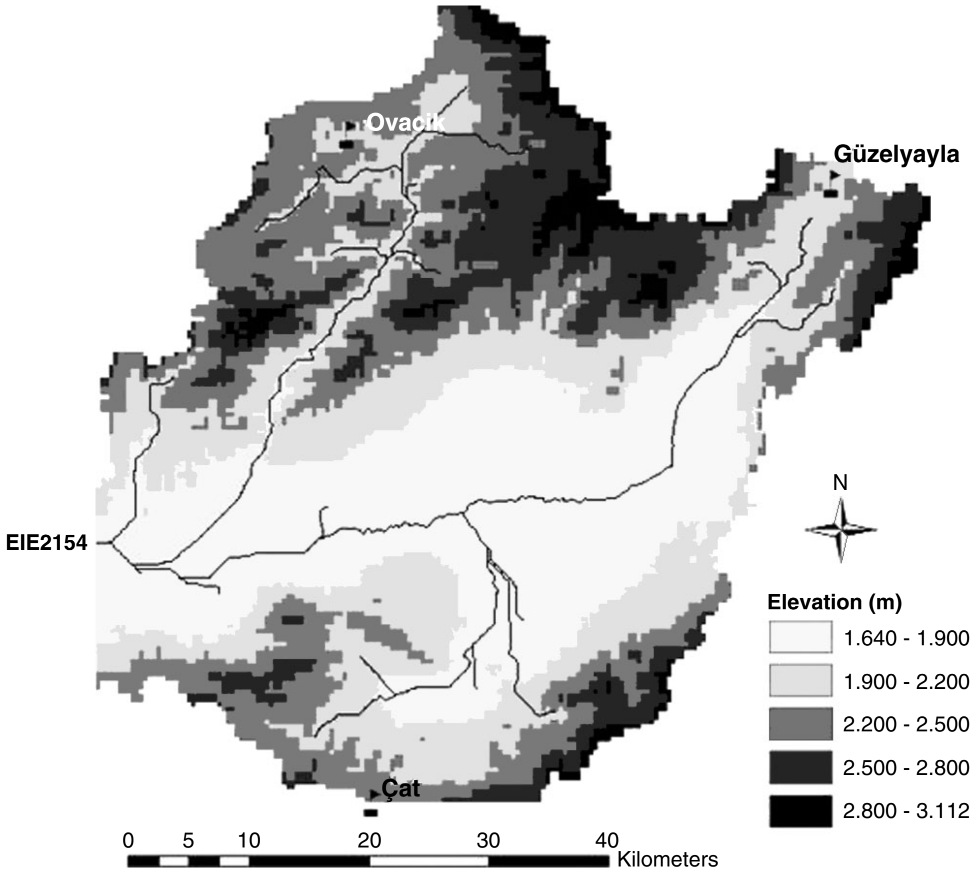

Figure 2. Locations of snow, meteorological and runoff stations on the upper Karasu basin

aim of understanding the behaviour of streamflow in this basin, a major objective of the present study is to apply a physically based, energy balance snowmelt model (Şensoy, 2005).

SNOBAL MODEL AND ITS APPLICATIONS

The model used to simulate the accumulation and melt of snow is called SNOBAL (Marks, 1988; Marks and Dozier, 1992; Marks *et al*., 1999b). It is available within the Image Processing Workbench (IPW) software package (Marks *et al*., 1999a). It is a point energy balance model that has been previously applied to locations in a wide range of systems (i.e. maritime, mid-latitude continental, continental maritime and boreal environments; Link and Marks, 1998; Marks *et al*., 1998). The snowpack's energy balance and associated melt, refreezing and water percolation are represented by a two-layer system, with a thin surface layer of fixed thickness and a lower layer of variable thickness. This approach allows adequate representation of rapid changes in the thermal status of the snowpack surface layer without the computational expense of a fully vertically distributed model (Anderton *et al*., 2002). Table I presents the state variables and forcing variables required by the SNOBAL model. State variables are input as initial conditions and then predicted by the model during the run. The model is then driven by the independent input of forcing variables to predict the state variables.

Copyright © 2006 John Wiley & Sons, Ltd.

Table I. State variables predicted by the model and forcing variables required by the model

State variables	Forcing variables
Snow depth (m)	Precipitation (mm)
Snow density (kg m^{-3})	Net solar radiation (W m^{-2})
Snow surface layer temperature (°C)	Incoming thermal radiation (W m^{-2})
Average snow cover temperature (°C)	Air temperature (°C)
Average snow liquid water content (%)	Vapour pressure (Pa)
	Wind speed (m s^{-1})
	Soil temperature (°C)

The model was applied to three representative sites in the upper Karasu basin, namely Güzelyayla (GY), Ovacık (OVA) and Çat (CAT). GY station (2065 m) is located on the northeast edge of the basin, and the general climatological conditions indicate that it is a cold, dry and windy site. OVA (2130 m), located on the north-northwest edge of the basin, is a cold and dry site. CAT (2340 m) is the highest automatic weather station (AWS) in Turkey, and it is at the south boundary of the basin. Both GY and CAT have an unobstructed fetch in the prevailing wind direction of northeast to southwest.

There are a total of five model applications: GY applications during 2002–04 and OVA and CAT applications for the 2003–04 snow season. Therefore, there are three temporally distributed point model applications at one site (GY for 2002–04) and the areal evaluation of three point applications for one snow season (GY, OVA, CAT for 2003–04 snow season). In all of these applications, a 2 h computational time step was used.

INSTRUMENTATION

Although there is a considerable amount of snow in eastern Turkey, the existing data infrastructure indicated that it was necessary to collect additional data for model applications. The decision was made to instrument a new station (GY), which then was supplemented by upgrading of others (OVA, CAT) and, most importantly, for data to become transferable in real time. These station locations were chosen to cover the range of characteristics (i.e. distributed over the basin at different elevations and climatic conditions) that can be observed in this mountainous region of the world, where the canopy effect is negligible, considering in addition the completeness and availability of meteorological data for model forcing.

Table II gives information on the AWSs along with their respective climate data measurements. The data collection program consisted of continuous automated measurements of a number of hydrometeorological variables at AWSs and manual snow surveys carried out with snow tubes monthly or bimonthly around the AWSs. Even the most common meteorological parameters are difficult to measure continuously at a remote site, because recording equipment exhibits varying degrees of instability depending on the environmental conditions.

The measurements of albedo, atmospheric/terrestrial longwave radiation and lysimeter yield are pioneer applications in Turkey. The new measurements enable the development of a high-quality time series of integrated climate data and the evaluation of the components of the energy balance of the snow cover.

ENERGY AND MASS BALANCE CALCULATIONS

In a seasonal snow cover, metamorphic changes and melting are driven by temperature and vapour density gradients within the snowpack, which are caused by heat exchange at the snow surface and at the snow–soil

Copyright © 2006 John Wiley & Sons, Ltd.

Table II. Instrumentation at the sites[a]

	Snow data (sensor models)	Radiation (sensor models)	Climate data (sensor models)	Data transfer
Güzelyayla (GY) (2065 m)	SWE (Sensotec) Snow depth (Judd) Lysimeter	Net (0·3–100 μm) (Kipp & Zonen (NR Lite)) Solar, albedo (0·3–2·8 μm) (Kipp & Zonen (CM3))	Precipitation (Met One) Temperature (Vaisala) Wind speed and direction (Met One) Humidity, air pressure (Vaisala)	Cable
Ovacık (OVA) (2130 m)	SWE (Druck) Snow depth (Judd)	Solar, albedo (0·3–2·8 μm) (Kipp & Zonen (CM3)) Longwave (in/out; (5–25 μm) (Kipp & Zonen (CG2))	Precipitation (Met One) Temperature (Vaisala) Wind speed (Young) Humidity (Vaisala)	Cable
Çat (CAT) (2340 m)	SWE (Druck) Snow depth (Judd)	Net (0·3–100 μm) (Kipp & Zonen (NR Lite)) Solar (0·305–2·8 μm) (Kipp & Zonen (CM3))	Temperature (Vaisala) Wind speed and direction (Met One) Humidity (Vaisala) Air pressure (Vaisala)	Inmarsat

[a] Commercial names are listed for information purposes only and are neither an endorsement nor a critique by the authors.

interface. In general, the energy balance of a snow cover is expressed as

$$\Delta Q = R_n + H + L_v E + G + M \quad (1)$$

where ΔQ (W m^{-2}) is change in snow cover energy, and R_n, H, $L_v E$, G and M (all W m^{-2}) are net radiative, sensible, latent (L_v is the latent heat of vaporization and E is the mass of water evaporated or condensed), ground (conductive) and advective energy fluxes respectively.

SNOBAL simulates each component of the snow cover energy balance and accumulates mass and thermal conditions for the next time step. It predicts melt in two snow cover layers and runoff from the base of the snow cover, and it adjusts the snow cover mass, thickness and thermal properties at each time step. If the computed energy balance is negative, then the cold content increases, and the layer temperature decreases. If the energy balance is positive, then the layer cold content decreases until it is zero. Additional input of energy causes the model to predict melt. If melt occurs, then it is assumed to displace air in the snow cover, causing densification and increasing the average liquid water content of both layers. Liquid water in excess of a specified threshold becomes meltwater outflow.

MODEL INPUTS

Surface roughness

The effective snow surface roughness, required for the turbulent transfer calculations, has been shown to be a dynamic property that is dependent on wind speeds and microtopography of the snow surface (Andreas, 1987). It is difficult to measure and, therefore, is usually estimated based on values reported in the literature ranging from 0·0001 to 0·01 m (Anderson, 1976; Moore, 1983), depending on snow depths and conditions. It is a site-specific and dynamic value, and it is not possible to determine an exact value for these sites. Testing was done during the initial model application phase using the physically realistic values referred to in the literature. The trial that gave the best fit with the observations was assumed to be the correct value for roughness. Roughness length was set to 0·001 m for GY and CAT, but it was 0·0001 for OVA, where the wind speeds are low, since it has been found that the aerodynamic roughness increases with increasing wind speed due to the influence of the drifting snow (Marsh, 1999). Unfortunately, there is no previous research on sublimation of blowing snow at the site, and SNOBAL does not include an explicit parameterization for

Copyright © 2006 John Wiley & Sons, Ltd.

blowing snow; therefore, the decision on surface roughness length depends directly on the average wind speed values at the sites. Surface roughness affects turbulent fluxes, and turbulent fluxes usually comprise a small component of the overall snow cover energy balance; therefore, the seasonal simulation should be relatively insensitive to roughness length.

Precipitation data

The rates and volumes of snowfall are very difficult to evaluate from precipitation gauge records (without heater) because they are affected not only by wind, site characteristics and precipitation intensity but also by variations in the density and structure of the snow crystals as they fall. Since the sites are cold (and windy for GY and CAT), there is an undercatch and freezing problem for snowfall; the recorded values are unrealistically small compared with snow depth and SWE at the stations and snowfall values of other stations. This underestimation is improved by the information gathered from the snow data measured with snow pillows and also from the nearby microclimatologic stations.

One common way of dealing with this is to use the change in SWE values for precipitation computation (e.g. method for editing precipitation data used by Garen and Marks (2001)). Such an analysis was carried out with the data provided from the GY site and the surrounding meteorological stations. The data acquired from another station that shows similar patterns with GY in terms of snow depth, SWE and air temperatures provided verification for the precipitation analysis at GY. First, daily precipitation amounts were computed according to changes in SWE (with some appropriate data quality checks and editing), then a simple fractioning approach was used to disaggregate the daily fields into 2 h fields. Precipitation values were corrected and computed for OVA and CAT with the same methodology.

Net shortwave radiation

Net shortwave radiation is the incoming radiation minus that reflected from the snow surface. The snow albedo, therefore, is a key parameter affecting the net shortwave radiation, as it defines how much of the incoming solar radiation is reflected from the surface. The snow albedo shows seasonal and daily variations depending on a wide variety of factors, like solar zenith angle, aging, wetness, impurity content, particle size, snow density and composition, surface roughness, cloud cover and spectral composition. Albedo is continuously observed at GY, except for the first winter (2002), with a set of pyranometers that are used to measure solar radiation and reflection in the range 0·305–2·8 μm.

It was decided to replace the physically based algorithm of albedo computation (dependent on snow grain size and sun angle) usually used with the SNOBAL model (i.e. the module ALBEDO in the IPW software package; Marks *et al.*, 1999a) with a new parameterized scheme developed specifically for the site using the observed data for the 2002–03 snow season, since there is a lack of measured data either for albedo or grain size. This scheme is based on a scenario using both a linear parameterization (Equation (2)) derived from principal component analysis (PCA) and an albedo decay function determined from aging (Equation (3)). PCA was applied to the observed data at GY for the 2002–03 snow season, which led to the selection of snow depth, global radiation and temperature as predictor variables, then stepwise regression was used to derive coefficients for normalized variables. The second equation is simply based on snow aging. The two equations were applied depending on the occurrence (Equation (2)) or non-occurrence (Equation (3)) of snowfall. The model results are shown in Figure 3; observed and modelled albedo values are presented both in 2 h and in daily time steps, besides the linear relationship and best fit with the daily data for the melting period of 2003 at GY. The same modelling approach was also used for CAT, where there is no albedo measurement during the model application of the 2003–04 snow season.

$$\text{Albedo} = 0{\cdot}75 + 0{\cdot}185d - 0{\cdot}1S_{\text{i}} - 0{\cdot}0001T_{\text{air}} \tag{2}$$

$$\text{Albedo} = 0{\cdot}77 - 0{\cdot}15\ln(t) \tag{3}$$

Copyright © 2006 John Wiley & Sons, Ltd.

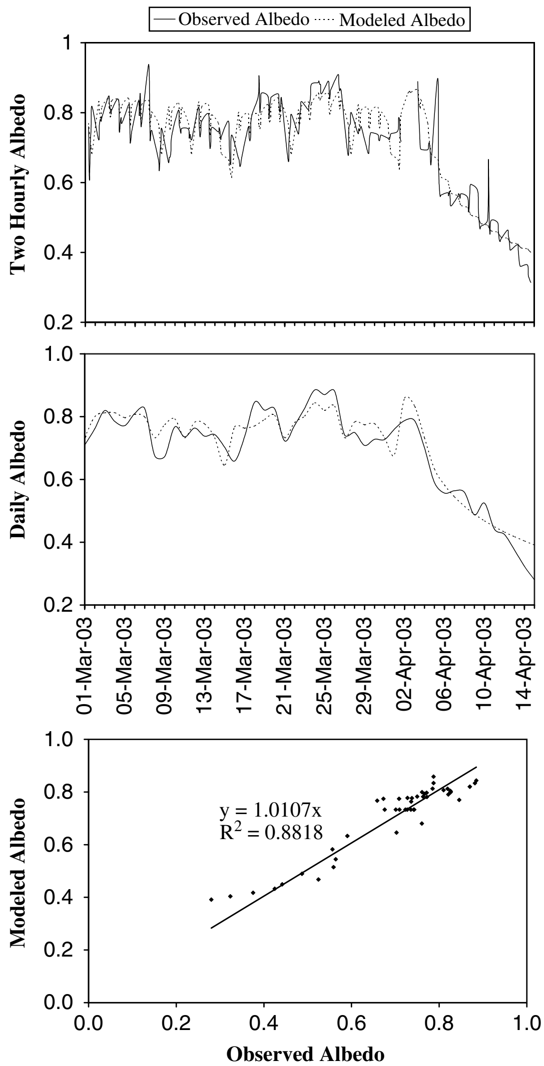

Figure 3. Observed and modelled albedo values for 2003 snowmelt period, GY

where d is snow depth, S_i is the global radiation and T_{air} is the air temperature, all of which are normalized and, therefore, are unitless; t (days) is aging time from the last snowfall. The albedo values thus estimated were used to determine the reflected shortwave radiation, which was subtracted from the measured incoming radiation to obtain net shortwave radiation.

Incoming longwave radiation

There is no measured incoming thermal radiation at GY and CAT stations; therefore, the snow surface temperature was computed as a residual. Snow surface temperature is difficult to measure by physical thermometry, but Davis *et al*. (1984) showed that the near-surface temperature of the snow tends to follow the air temperature. This occurs because the insulating characteristics of the snow cover allow the surface layer to come into temperature equilibrium with the atmosphere even though this may create large temperature differences between the surface and lower layers.

Copyright © 2006 John Wiley & Sons, Ltd.

Since the snow surface temperature values were measured manually for a brief period of time at GY and OVA stations, a linear relation between air and snow surface temperatures was developed using 43 observations, with $r^2 = 0{\cdot}89$:

$$T_{\text{snow}} = 1{\cdot}02T_{\text{air}} - 3{\cdot}17 \tag{4}$$

where T_{snow} (°C) is the snow surface temperature and T_{air} (°C) is the air temperature, with the constraint of maximum $T_{\text{snow}} = 0\,°\text{C}$. Incoming longwave radiation is calculated using measured net radiation values as

$$L_{\text{i}} = R_{\text{net}} - S_{\text{net}} + \varepsilon_{\text{snow}}\sigma T^4_{\text{snow}} \tag{5}$$

where L_{i} (W m^{-2}) is the incoming longwave radiation, R_{net} (W m^{-2}) is the net radiation, S_{net} (W m^{-2}) is the net shortwave radiation, $\varepsilon_{\text{snow}}$ is the emissivity of the snow surface (0·99), T_{snow} (K) is the snow surface temperature and σ is the Stefan–Boltzmann constant ($5{\cdot}67 \times 10^{-8}$ W m^{-2} K^{-4}).

Net longwave observations at OVA were used to check the snow surface temperature computations. Snow surface temperature values were computed from measured terrestrial longwave radiation ($T_{\text{snow-observed}}$) and then compared with the results of the empirical formula ($T_{\text{snow-modelled}}$) (Equation (4)). Figure 4 presents the relation between air temperature T_{air} and snow surface temperature in terms of both the observed values with the pyrgeometer ($T_{\text{snow-observed}}$) and computed ones derived from the empirical formulation of manual measurements ($T_{\text{snow-modelled}}$). Although there is considerable scatter in the relation between the two data sets, a strong correlation is found between them. According to these graphics, the empirical equation adequately represents the snow surface temperature values overall (the first graphic in Figure 4); however, it may be more appropriate to separate the equation into two parts, one for the afternoon hours (12 : 00–16 : 00) at which the air temperatures will be relatively high (the last graphic in Figure 4) and one for the rest of the day (the second graphic in Figure 4), for which the equation explains about 90% of the relation. The main discrepancies occur when the air temperature is above freezing, since the snow surface should be at freezing when the air temperature is higher (Shusun *et al.*, 1999).

Although several longwave radiation models have been developed (e.g. Satterlund, 1979; Idso, 1981), and these models can successfully represent daily average atmospheric longwave radiation with cloud cover correction, they are not adequate to represent diurnal variations for a 2 h computational time step. Therefore, it was preferred to use snow surface temperature data together with observed radiation values to compute incoming longwave radiation as a residual (Equation (5)) instead of other empirical models.

Air temperature, vapour pressure and wind speed

Vapour pressure for the individual sites was computed from site air temperatures and relative humidity values using standard meteorological algorithms. In contrast to GY and CAT, where average wind speeds are around 3·5 m s^{-1} and 4 m s^{-1} respectively during the snow season, wind speeds are lower at OVA, with an average of 1·5 m s^{-1}. OVA is also distinct in that its temperatures are cooler than one would expect based on its elevation and the temperature trends based on the other sites.

Soil temperature

Since the sites appear to be cold and sometimes have a shallow snowpack, setting the soil temperature to a constant of 0 °C is not a feasible assumption, since this led to an unrealistically high simulated heat transfer from the soil to the snow. Therefore, the soil temperature data from another station with similar snow accumulation and melt patterns were used for soil temperatures at 20 cm depth.

Although the model was applied in 2 h time intervals, the climate input data are presented in 5-day averages for clearer illustration in Figure 5. The model applications have shown that the initiation of snowmelt and the melt rate are very sensitive to relatively minor changes in climate forcing. To simulate the snow cover processes correctly, it is essential to use forcing data that account for these minor variations.

Copyright © 2006 John Wiley & Sons, Ltd.

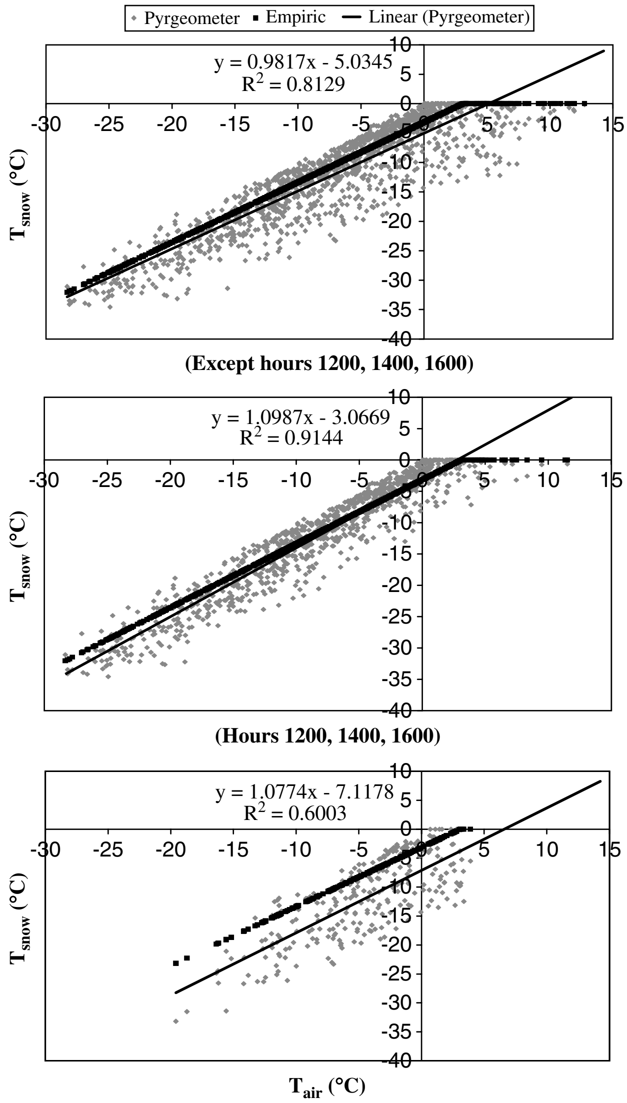

Figure 4. Snow surface ($T_{\text{snow-observed}}$ by pyrgeometer, $T_{\text{snow-modeled}}$ by empirical formula) and air temperature T_{air} relations, OVA, 2004

MODEL OUTPUTS

The results are analysed under two main topics with two more subtopics under each. The first topic is the temporal analysis of the point applications at one station for three consecutive snow seasons, and the second is the areal analysis of the point applications at three stations for one snow season. Each analysis is further evaluated both in terms of snow cover energy balance and in terms of snow cover mass balance.

Temporal analysis of point applications

Compared with the long-term averages, including manual snow course measurements at GY, OVA and CAT between the years 1976 and 2003, the first two snow seasons were average years, whereas SWE values were well above average during the peak period of 2004. Although there are similarities between snow seasons in terms of snowfall, melt patterns have different characteristics for each year. The removal of snowpack from

Copyright © 2006 John Wiley & Sons, Ltd.

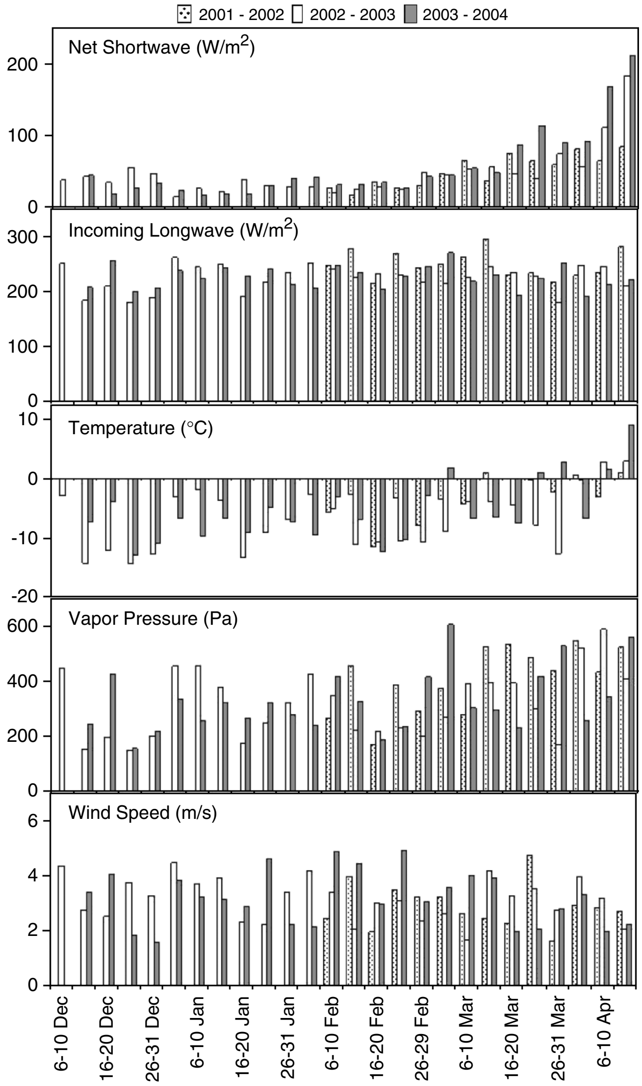

Figure 5. Model input parameters at GY during 2002–04 snow seasons

GY occurred within the interval of 10–15 April for all 3 years. However, the snow covered area images from satellites (NOAA and MODIS) indicated gradual melting for the year 2004, especially at the high elevation zones, in contrast to the sharp melting period observed for the year 2003.

Snow cover energy balance. Figure 6 depicts energy flux outputs in 5-day averages for each season, including net radiation, turbulent energy (includes both sensible and latent heat fluxes), ground heat flux and total energy; advective energy is not shown because it is very small in amount. Below, simulations for each of the 3 years at GY are analysed in detail.

2001–02, GY: Snowmelt runoff started in the 1–5 March 2002 time period with an increased net radiation effect. Gradual melting developed continuously until 15 April, with net radiation and turbulent heat fluxes dominating. The greatest negative net turbulent heat fluxes occurred within the period of 6–10 March. The

Copyright © 2006 John Wiley & Sons, Ltd.

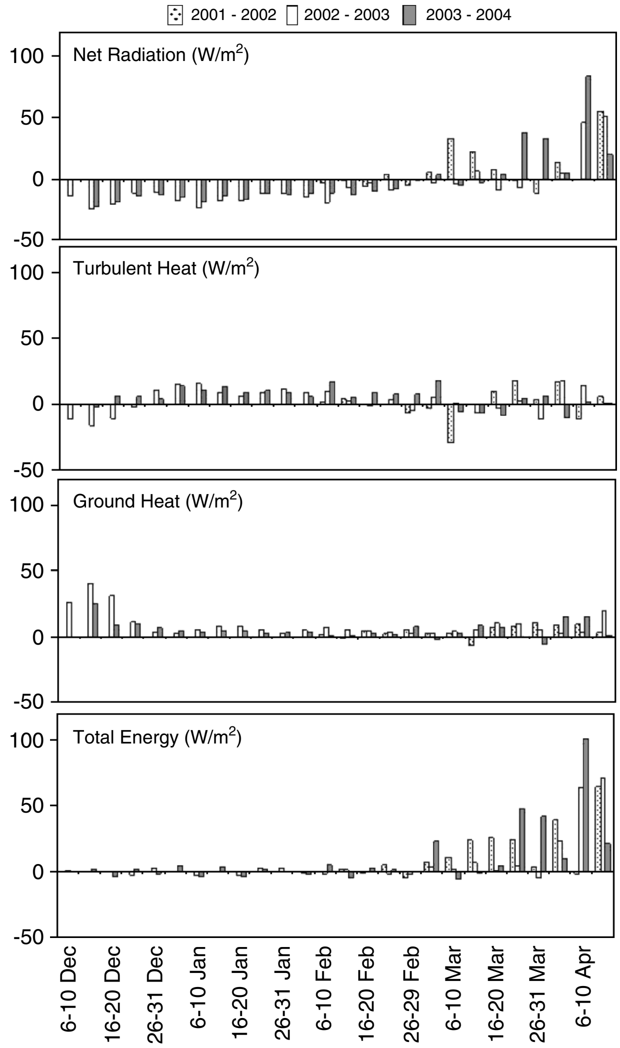

Figure 6. Model outputs for energy flux terms at GY during 2002–04 snow seasons

basic reason is the climate conditions on 9 March, on which 8·25 m s^{-1} wind speed was observed, although the average wind speed for the 5-day period was 2·62 m s^{-1} (Figure 5). On this day, the vapour pressure was very low, around 200 Pa, and the average temperature decreased by 5 °C. Under these conditions, both the sensible and latent heat fluxes were generally negative, since the air was both colder and less humid than the snow surface, and the high wind speed enhanced this negative turbulent heat flux. During the period 11–15 March, air temperatures turned to positive values, and there was significant cloud cover, resulting in the highest incoming longwave radiation for the season (Figure 5). A sudden increase in wind speeds during 21–25 March coincided with a reaccumulation of snow and also directly affected sensible heat flux, since the air temperatures were around 0 °C. Both the sensible and latent heat fluxes were generally positive during this period; together, these explain more than 50% of the total energy for snowmelt during this interval (Figure 7). Precipitation falling as snowfall during 6–10 April caused a sharp latent heat flux increase, which explains half of the total energy. Finally, for the last interval, ΔQ yielded an amount of melt due to high net radiation, which was around 80% of the total energy.

Copyright © 2006 John Wiley & Sons, Ltd.

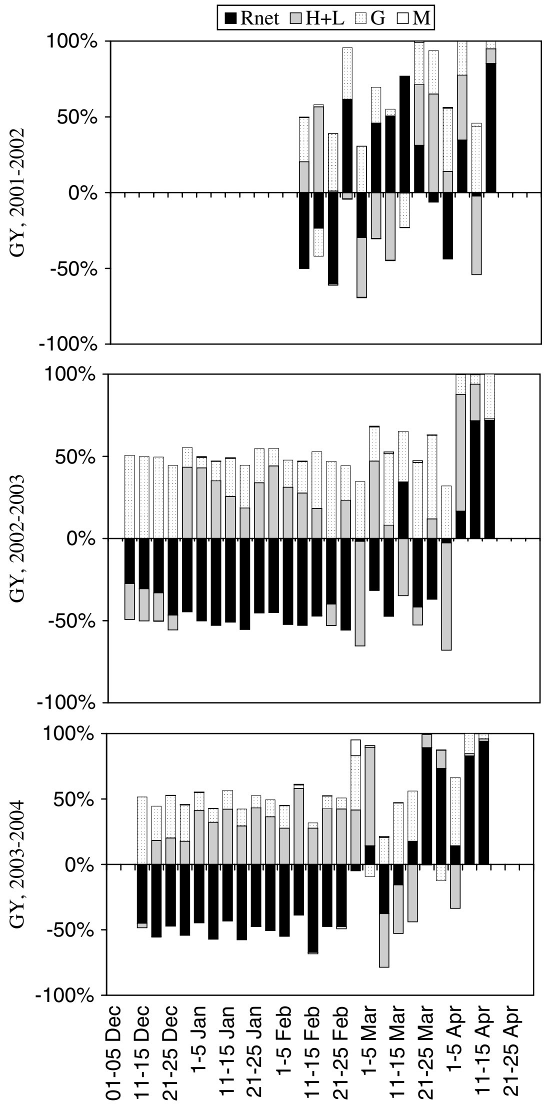

Figure 7. Energy percentages within the total energy at GY

2002–03, GY: Sensible heat fluxes oscillated in direction during the snow season, whereas latent heat fluxes tended to be negative through the season, indicating evaporative cooling of the snow cover. Since the site is dry and cold, observed sensible and latent heat fluxes were small in amount, although the wind speeds were rather high, averaging a little over 3 m s^{-1}. In contrast to the 2001–02 snow season, accumulation was continuous until the beginning of April 2003, and then a sharp ablation period started on 3 April, ending on 15 April. Increases in average air temperature and wind speed, from $-12{\cdot}7$ to $-0{\cdot}2\,^{\circ}C$ and from 2·7 to 3·9 m s^{-1} respectively (26–31 March to 1–5 April), led to a drastic increase in sensible heat flux, which initiated the snowmelt. From then on, net radiation constituted around 70% of the overall energy (Figure 7).

2003–04, GY: The accumulation period continued until an unusual flood event occurred during 29 February–6 March 2004 due to increased turbulent flux and rain on snow (ROS). The precipitation in the form

Copyright © 2006 John Wiley & Sons, Ltd.

of rainfall, due to positive air temperatures, contributed to positive advective energy and, more importantly, caused an increase in the specific mass of the existing snow cover. Turbulent heat flux increased to 76·3% of the total energy (Figure 7), which is the maximum value of all 3 years. Similarly, advective energy increased to 2·17 W m^{-2} at the end of February. Higher temperatures and vapour pressures increased the net turbulent heat, which led to melting of the already isothermal snow. As the event ended and conditions cleared, there was a sharp drop in incoming longwave radiation. After the cold and cloudy period, the snowmelt restarted on 22 March at a much more moderate rate with the net radiation dominating. During the next 5 days, temperatures decreased, accompanied by high winds, resulting in rather low turbulent heat. Finally, with the net radiation increase, snow cover disappeared on 11 April.

In summary, the year 2002 was different from the other 2 years, with an early melt as a result of solar radiation and an extensive melt period of approximately 1·5 months. The year 2003 was distinguished by a sharp and short melt period, starting with high turbulent heat and continuing with high net radiation, ending almost within 10 days. The year 2004 was characterized by a flood due to high turbulent heat fluxes and an ROS event. The timing of snowmelt is comparable for the last 2 years except for the ROS event.

Snow cover mass balance. Simulated snow cover mass is compared with measured mass in terms of both SWE and snow depths (Figure 8a–c) for model verification in 2 h time steps. The model converts rain directly to runoff when no snow cover is present. When snow is present, runoff is the sum of melt, less the liquid water holding capacity of the snow, plus rainfall. Early in the spring, the model simulated several minor melt events that do not exceed the water holding capacity of the snowpack at the site. Model simulation results are in close agreement with the continuous snow pillow data throughout the snow season, except for some discrepancies due to accuracy issues with the snow pillow observations, as described below.

The continuous automatic depth measurements are used to validate the simulated snow depths (Figure 8a–c). Although the total change in snow depth is modelled well over the whole snow season, there are periods when the model seems both to over- and underestimate the snow depths. In addition, mean depth measurements recorded manually during bimonthly snow course surveys provided an additional validation data set. Wind speed values greater than 6·5 m s^{-1} are also plotted to show its effect on redistribution of snowfall during the accumulation phase. The deviations between the model results and the measured snow depth (also SWE) are observed during the pronounced windy periods, since the model does not include an explicit parameterization for blowing snow.

Snow lysimeters are used to provide a physical measurement for testing models of snowpack energy balance and/or meltwater production (Kattelman, 2000). Therefore, the simulated snowmelt runoff values are also compared with measured yield/discharge from the lysimeter for the years 2003 and 2004 at GY. Figure 9 shows time series of observed and modelled meltwater outflow from the base of the snowpack for the year 2003.

Two snowmelt test periods, 5–10 April 2003 (SM-I) and 11–14 April 2003 (SM-II), are examined below. During SM-I, a significant reduction in SWE occurred with an increase in lysimeter discharge. There is a time lag of approximately 1 day for the lysimeter to start yielding; although it is possible that there are errors in how SNOBAL handles the delay of meltwater as it flows through the snowpack, known problems with the lysimeter (such as freezing) make this the more likely error source. Nevertheless, the lysimeter melt rates are comparable to the modelled rates (Figure 9b). Following a cold period with little melt on 4 April, daily peak outflow magnitudes rapidly increased to over 3 mm h^{-1}, with very sharply peaked daily hydrographs. The timing of modelled outflow is generally excellent for both the peaks and troughs for the following days. There is a discrepancy, however, in the magnitudes of modelled and observed values. During SM-II, the lysimeter did not indicate any corresponding significant yield increase. A number of reasons can be stated for the different lysimeter responses between SM-I and SM-II. One reason may be a tipping-bucket failure due to extensive melting and rainfall followed by a period of rainfall on 8–10 April. Other reasons could be:

Copyright © 2006 John Wiley & Sons, Ltd.

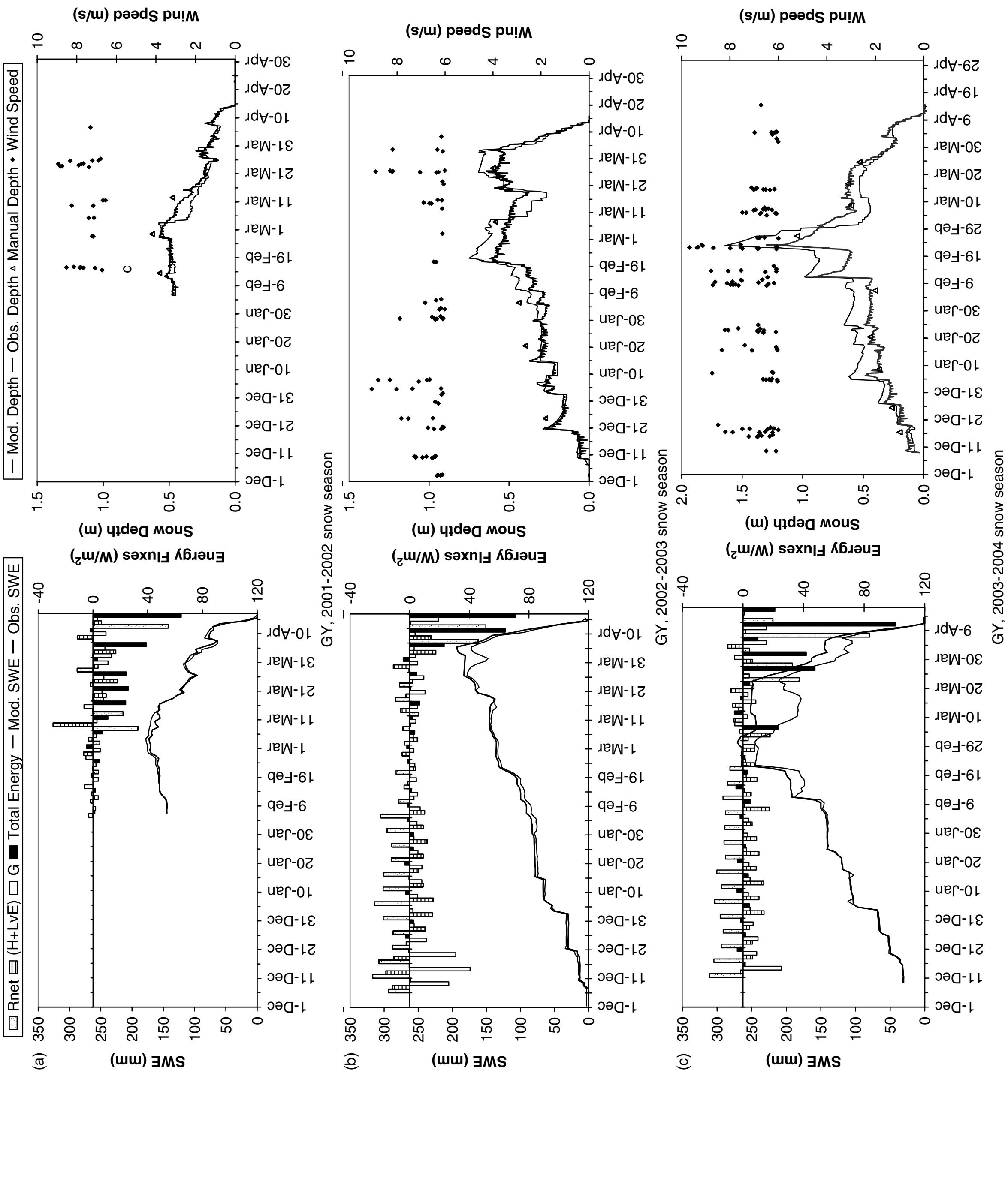

Figure 8. Simulated and observed snow data along with energy fluxes and wind speeds: (a) GY, 2001–02 snow season; (b) GY, 2002–03 snow season; (c) GY, 2003–04 snow season; (d) OVA, 2003–04 snow season; (e) CAT, 2003–04 snow season

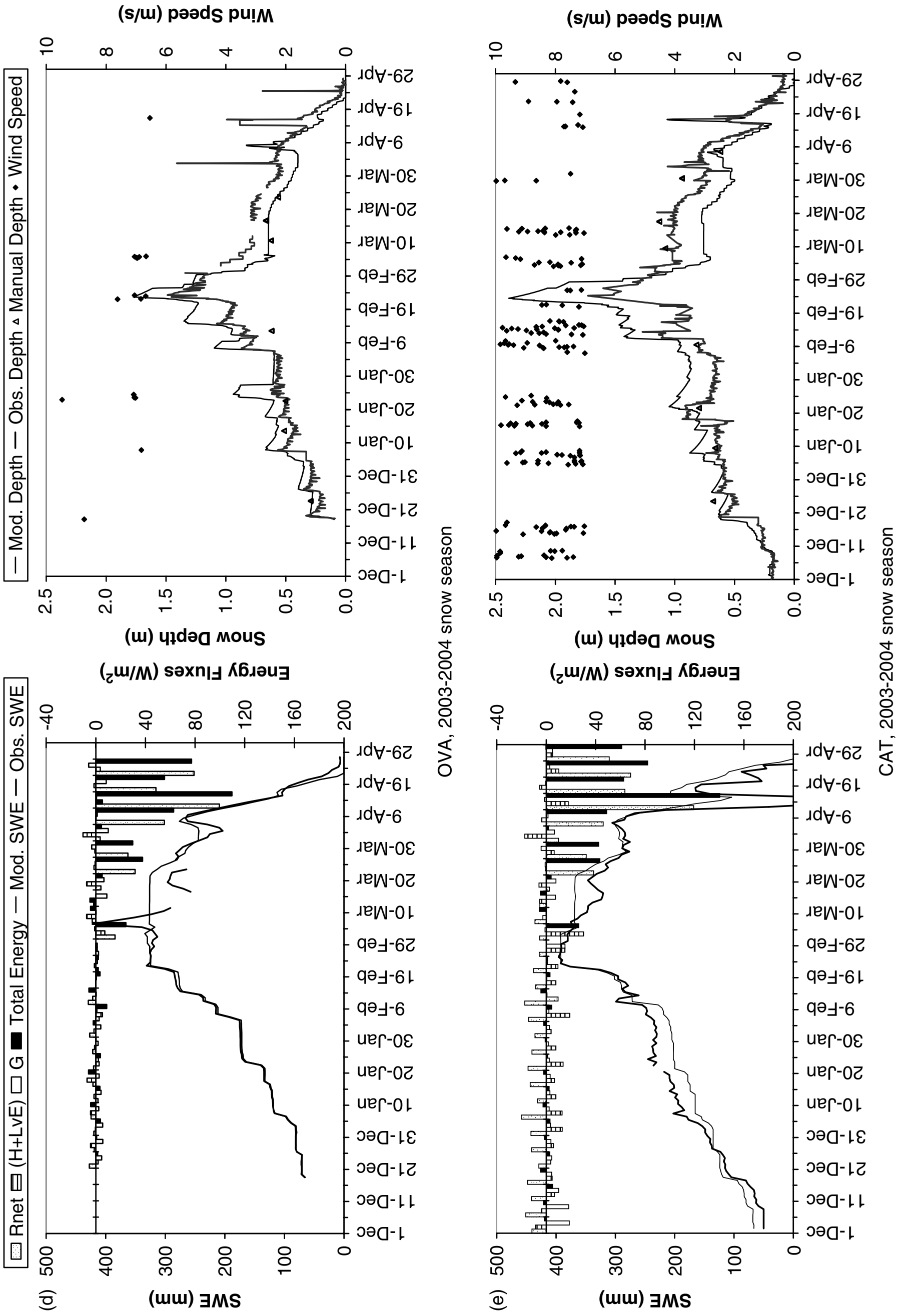

Figure 8. (*Continued*)

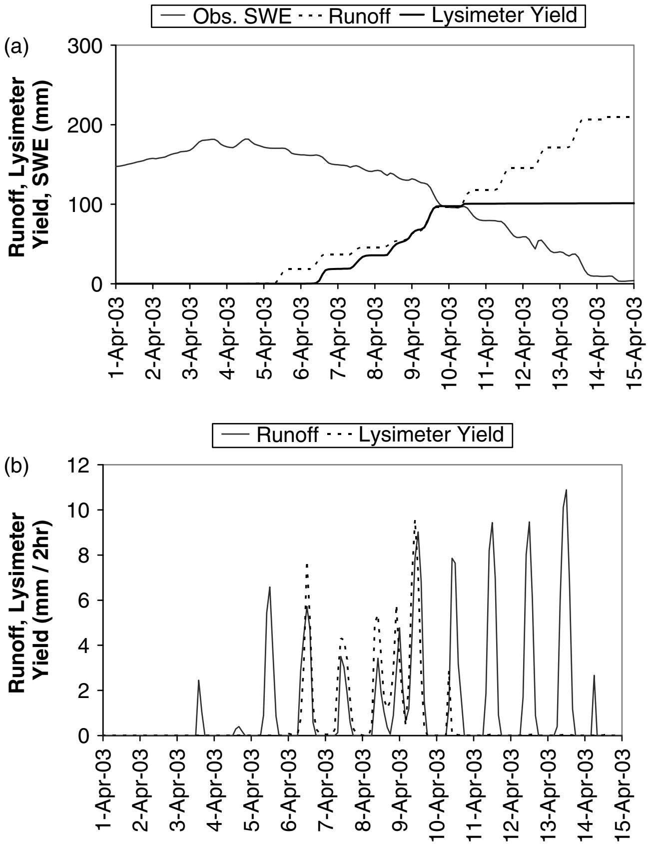

Figure 9. (a) SWE, cumulative modelled runoff and lysimeter yield, GY, 2003. (b) Two-hourly rates of modelled runoff and lysimeter yield, GY, 2003

1. The non-uniformity of snow depth distribution within the snow station; thus, the lysimeter might have a snow depth that is less than that on the snow pillow.
2. The difference between the areas of the lysimeter (1·53 m^2) and snow pillow (6·50 m^2) may be another reason for the different lysimeter responses between SM-I and SM-II.
3. The difference in the material between the lysimeter (galvanized steel) and the snow pillow (hypalon) might have resulted in an increased evaporation rate from the lysimeter (Tekeli *et al*., 2005).

A plot of observed and modelled cumulative basal meltwater outflow (Figure 9a) clearly illustrates the differences. Since similar problems were encountered, results are not presented for the year 2004.

Areal evaluation of point applications

From the SWE graphs (2003–04), it can be seen that the whole snow season can be broken into segments based on climatic conditions (Figure 8c–e). The snow cover development occurred during the period from 1 December 2003 to 29 February 2004. A series of cold storms deposited significant amounts of snow on 10–11 February and 21–22 February; 16–25 February was one of the coldest periods through the whole snow season, with temperatures well below freezing (−10 to −20 °C) and high wind speeds observed at all the stations; 22–29 February was a very cold, fairly clear period. See Figure 10 for input data categorization.

The 29 February–6 March event was accompanied by high winds and intense rainfall, which was one of the most intense ROS events ever recorded. The station at the Erzurum airport reported rainfall of about

Copyright © 2006 John Wiley & Sons, Ltd.

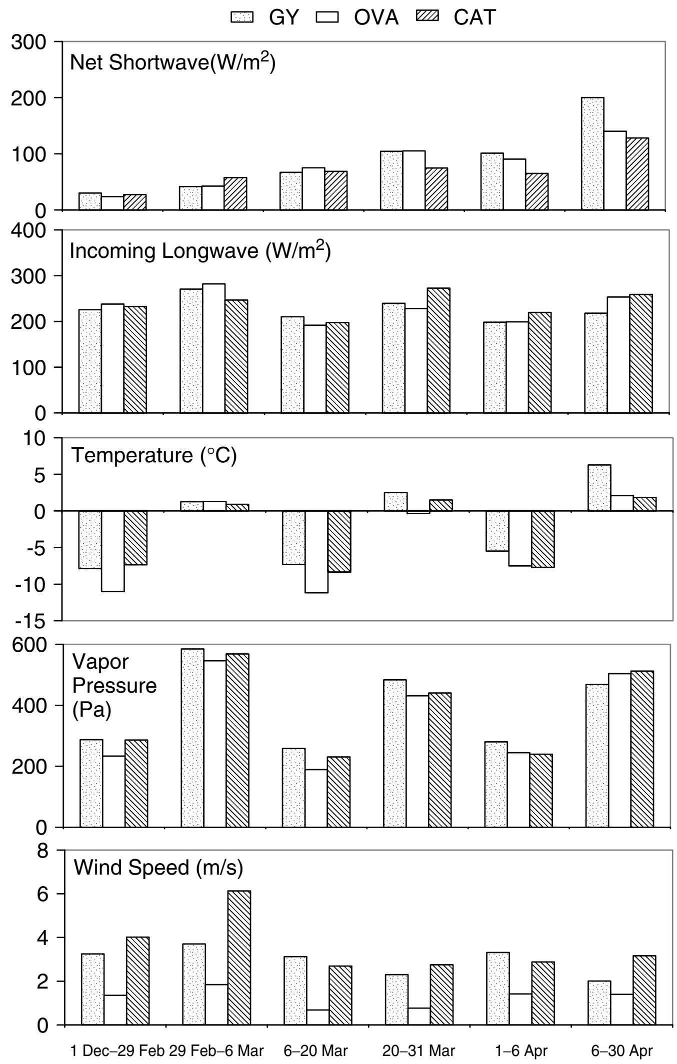

Figure 10. Model input parameter categorization at GY, OVA, CAT, 2003–04 season evaluation

50 mm during the event. Intense rainfall combined with rapid snowmelt contributed to the flood event. Peak flows on headwater streams and rivers draining the upper Karasu basin (station 2154) occurred on 6 March 2004, when the river rose from 10 m^3 s^{-1} on 29 February to 120 m^3 s^{-1} by 6 March.

Low air temperature, vapour pressure and solar radiation clearly indicate the period for the development of snow cover (1 December–29 February). In contrast, climate conditions during the ROS event show a reduction in solar radiation, air temperature always above freezing and an increase in vapour pressure to near or above the saturated vapour pressure at 0 °C. During the ROS event, air temperatures were above freezing, and there was a large humidity gradient towards the snow cover at all three sites (which can be observed from hourly data).

Snow cover energy balance. A few minor deposition events occurred during the last week in October and the last week in November, but these melted rapidly and did not persist for more than 2 or 3 days. During the snowpack development phase, the net turbulent flux fluctuated between 0 and 10 W m^{-2} at GY and CAT

Copyright © 2006 John Wiley & Sons, Ltd.

(Figure 11). In contrast, it was around zero at OVA, where L_vE and H displayed the common characteristic during non-storm periods that they were of the same magnitude but opposite in sign. Thus, total energy remained around zero, with the dominating negative effect of net all-wave radiation during this snowpack development phase (1 December–29 February; Figure 11).

During the ROS event (29 February–6 March), the snow cover energy balance was quite different, as all sites had a distinctly positive energy balance with a large input of turbulent energy (Figure 11). Both the sensible and latent heat fluxes were positive and combined to enhance the snow cover energy balance significantly. Turbulent fluxes constituted around 85% of total energy at GY and CAT for the period of 1–5 March, but this value was 30% for OVA (Figure 12). The advective energy became effective and significant for the first time in terms of percent of total energy (Figure 12). The result was that total energy was large and positive throughout the ROS event, providing a substantial amount of energy for snowmelt. Because of the influence of large volumes of 0 °C meltwater percolating into the soil column, the temperature gradient between the soil and the snow was removed, and ground heat flux was unimportant (Figure 11).

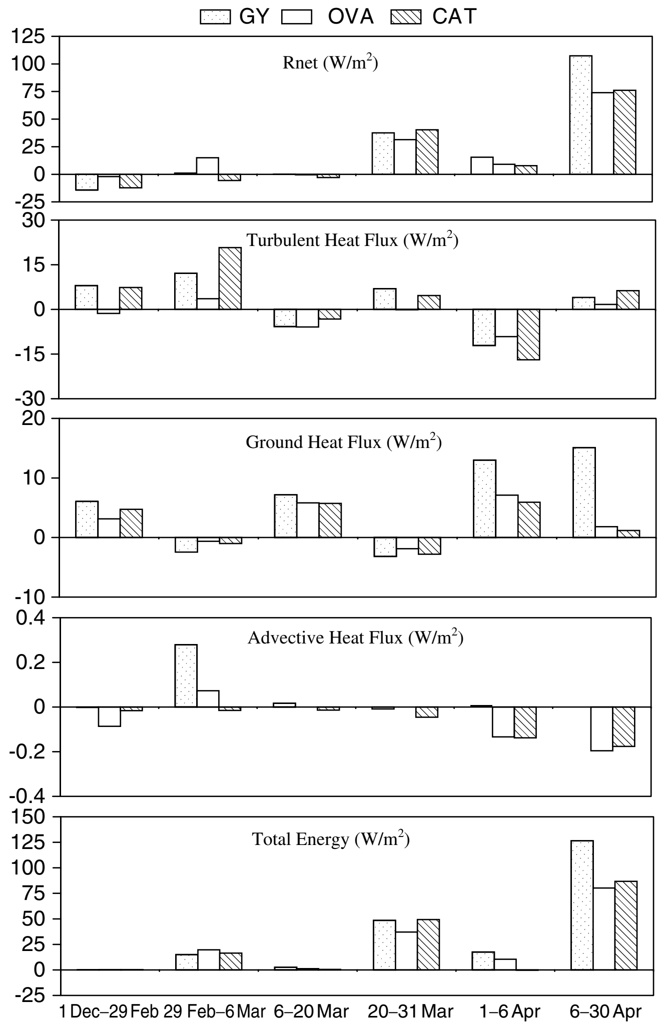

Figure 11. Model output categorization at GY, OVA, CAT, 2003–04 snow season

Copyright © 2006 John Wiley & Sons, Ltd.

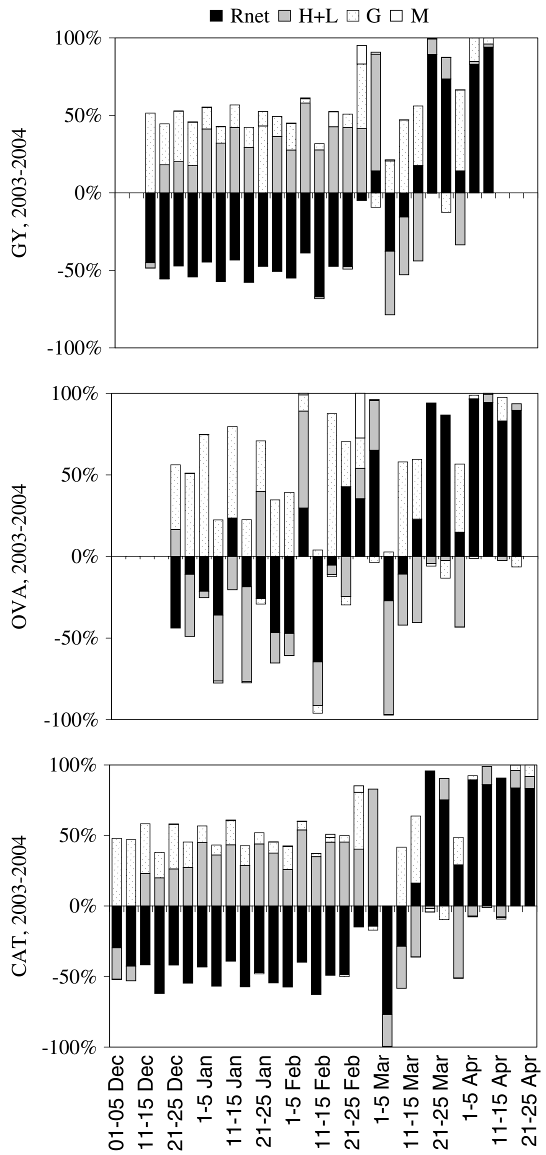

Figure 12. Energy percentages within the total energy (GY, OVA, CAT)

The total energy balance was again around zero during the period immediately following the ROS event, 6–20 March (Figure 11). Although the net solar energy had an increasing trend with the progression of the season, net longwave radiation values were high but negative due to low temperatures and vapour pressures; all of these caused net all-wave radiation to be zero. In addition, extreme cold conditions caused both the sensitive and latent heat fluxes generally to be negative, which led to large negative turbulent fluxes.

During the clear sky period of 20–31 March, the increased net solar radiation under clear skies dominated the energy balance and constituted around 80 to 95% of the total energy at the three sites; total energy during this period was effectively well above zero (Figure 12). The air temperatures were well above 0 °C, and positive turbulent heat fluxes were observed at GY and CAT, though negative turbulent heat occurred at

Copyright © 2006 John Wiley & Sons, Ltd.

OVA, most probably due to negative air temperatures. Cloudy skies with rather low temperatures and vapour pressures caused both the latent and sensible heat fluxes to be negative and constitute 50% of total energy fluxes (Figure 12) during the mixed ROS event on 1–6 April. The last part (7 April and onward) is purely a snow-melting period with the considerable effect of net solar radiation (Figure 11). Snowpack disappeared in mid-April at GY, whereas it extended until the end of April at OVA and CAT (Figure 8c–e).

Snow cover mass balance. Simulated SWE matched observed SWE (Figure 8c–e) very closely during the development of the snow cover, especially at GY and OVA, whereas there is a deviation for CAT, which is probably attributable to problems related to the snow pillow itself (see next section). In the same manner as the GY model application for 2003–04, there is a mismatch for the modelled and observed SWE values after the ROS period. The two gaps in the observed record of OVA might be due to problems related with improper functioning of the datalogger as a result of low temperatures.

The model has a tendency occasionally to estimate maximum snow depths exceeding the observations. This difference is not consistent between stations and is difficult to explain. Although it is possible that the model is in error due to inaccuracies in depicting snow density, it is more likely that the discrepancies are due to observation errors. For example, there are unrealistically high accumulation records (Figure 8d), especially at OVA. It is possible that the ultrasonic depth gauge (UDG) record is in error, and the observed inaccurate accumulation is due to refreezing of surface meltwater (which reduced the distance into the snowpack that could be detected) or the UDG is detecting the top of falling snow rather than the snowpack surface itself.

Melt with associated runoff production started during the first days of March and continued over a period different for each of the sites. The maximum sustained melt rate exceeded 6 mm h^{-1} at CAT, whereas it approached 5 mm h^{-1} for OVA and was 5·5 mm h^{-1} at GY. Melt rates at CAT were comparable to those at GY; however, a substantially larger snowpack at CAT resulted in an extended ablation period, with complete ablation occurring almost 2 weeks later than at GY.

SNOW PILLOW ERRORS

In general, snow pillows function adequately; however, long-term experience with snow pillows demonstrates that they can yield unpredictable and erroneous results that make it difficult for water resource managers and researchers to determine what is occurring (Johnson and Marks, 2004). There are error sources related to the snow pillow, such as a leaking pillow or the occurrence of ice bridging and a connection with the snowpack outside of the snow pillow causing a reduction of the measured pressure and calculated SWE. In addition, soil expansion is a real problem at the beginning of the snow season if rainfall occurred after the calibration of a snow pillow.

SWE sensor errors are most severe during the transition from a cold to a warm snow cover when the 0 °C isotherm progresses from the snow surface toward the ground. When the isotherm reaches the ground before reaching the sensor, heat from the ground can no longer be conducted into the snow, producing a sudden increase in the snowmelt rate. This can cause an SWE sensor overmeasurement error that continues to increase until the 0 °C isotherm reaches the top of the sensor (e.g. a sudden jump at OVA in Figure 8d).

Either under- or overmeasurement errors may occur at critical times when the snow cover transitions from winter to spring conditions and at the start of periods of rapid snowmelt. There was an unusual circumstance in early March 2004 in which precipitation fell as rainfall due to increased temperatures. Average daily temperatures increased from −13·4 to +3·4 °C. Over the next several days, average temperatures became very cold, down to −10 °C. Because the snow pillow alters the thermal and moisture exchange between the soil and snow, and because the soil was quite moist, it can be assumed that a significant transfer of vapour from the soil to the cold snowpack would have taken place prior to this ROS event. This vapour transfer could not have occurred over the snow pillow, so it can also be assumed that the snow over the snow pillow would be colder and may have contained basal ice. Rainwater was probably retained above the snow pillow

Copyright © 2006 John Wiley & Sons, Ltd.

until the thermal gradient was removed and the ice layers melted. At that time, a sudden reduction in SWE occurred, much like the breaking of an ice dam, which would explain the rapid large loss of SWE reported at the three stations (Figure 8c–e). Later manual snow samples indicated several very dense layers deep within the snowpack, as well as distributed ice lenses.

There is a similar pattern in the 2002–03 snow season simulation (Figure 8b): an amount of pre-melting within the time period of 11–20 March 2003 due to net radiation resulted in ice bridging. The pack was not isothermal at this time, and sustained melt did not occur, which caused the sidewalls to carry the ice load, thus decreasing the pressure on the snow pillow during 26 March–1 April 2003.

VALIDATION STATISTICS

Validation measurements included snow depth measured with an ultrasonic depth sensor, SWE from snow pillows, manual observations of SWE and snow depth, and meltwater outflow from lysimeters. Model performance itself can be judged by visual comparison of time series of observed values and modelled output (e.g. SWE, snow depth, runoff) and with quantitative measures of goodness of fit. Three standard quantitative tests are used to evaluate model performance and the goodness of fit for the model applications.

The root-mean-squared error (RMSE) between simulated and observed values and the mean bias difference (MBD), or mean deviation of simulated from observed values, are presented below. The Nash–Sutcliffe coefficient or 'model efficiency' (ME), which describes the variation in the observed parameter accounted for by the simulated values (Nash and Sutcliffe, 1970), is also presented for SWE. These tests were chosen to illustrate the difference between simulated and observed values rather than the error, because there is a significant uncertainty in the measured parameters (Marks *et al*., 1999b). RMSE and MBD are calculated for both SWE and snow depth for all the applications, disregarding negative records of SWE at CAT, as shown below:

$$\mathrm{RMSE} = \sqrt{\frac{\sum_{i=1}^{n}(x_{\mathrm{mod}} - x_{\mathrm{obs}})^2}{n}} \tag{6}$$

$$\mathrm{MBD} = \frac{1}{n}\sum_{i=1}^{n}(x_{\mathrm{mod}} - x_{\mathrm{obs}}) \tag{7}$$

$$\mathrm{ME} = 1 - \left[\sum_{i=1}^{n}\frac{(x_{\mathrm{obs}} - x_{\mathrm{mod}})^2}{(x_{\mathrm{obs}} - x_{\mathrm{ave}})^2}\right] \tag{8}$$

where x_{mod} is the modelled value, x_{obs} is the observed value and x_{ave} is the average value of the observations. Values of these validation statistics are presented in Table III. The magnitudes of RMSE and MBD in all

Table III. Statistical model evaluation

	SWE				Depth		
	RMSE (mm)	MBD (mm)	ME	Max. (mm)	RMSE (mm)	MBD (mm)	Max. (mm)
2001–02 GY	0·21	1·63	0·83	174·2	16	−2·22	577
2002–03 GY	0·18	3·50	0·86	184·0	18	2·53	641
2003–04 GY	0·68	15·7	0·58	273·5	42	6·31	1300
2003–04 OVA	0·49	0·56	0·80	335·0[a]	47	2·74	1488
2003–04 CAT	0·81	4·25	0·68	396·6	64	5·25	1728

[a] Taken from SNOBAL result.

Copyright © 2006 John Wiley & Sons, Ltd.

cases are small and not much more beyond the sensitivity of the snow pillow. A large bias error is apparent at GY for the 2003–04 snow season, since the ice-bridging problem was pronounced in the error calculation. This error is not so apparent for OVA and CAT, due to the lack of observed SWE data at OVA for that period, and since the ice-bridging problem was not as pronounced at CAT compared with the other stations.

Model performance can be evaluated as good according to such small differences between observed and modelled SWE and snow depths. Figure 8 shows that simulated snowpack follows the trends in measured SWE and snow depth with small RMSE values. Good agreement is also evident between the simulated and the manual depth measurements, which were chosen to be representative of overall snow conditions.

The wind effect is more pronounced during the 2004 winter than the others, which generates a difference between observed and simulated snow depth (and also SWE) values, especially after 12 February (Figure 8e). Under these conditions, the pattern of extensive snow deposition and drifting leading to the development of scour sites on wind-exposed areas should be investigated in future projects. This will improve understanding of the causes for the differences and help to define the critical processes that must be included in watershed-scale snow models (Marks and Winstral, 2001).

CONCLUSIONS

SNOBAL was selected as a suitable physically based layered snow process model, as it provides the necessary level of complexity to simulate accurately the timing and rate of meltwater outflow from the base of the snowpack with an energy and mass balance approach. Since the overall objective of this part of the study has been to investigate the effect of each energy flux on snow cover both during accumulation and during ablation, the model necessarily had to have a high temporal resolution, which was set to 2 h time steps. Net radiation fluxes were found to dominate the surface energy balance, representing about two-thirds of the energy input to the snowpack most of the time. This emphasizes the importance of correct estimation of longwave radiation and albedo when modelling melt. The work that was undertaken to model albedo and longwave radiation values is, however, site specific and cannot be generalized for the other parts of the region. Results from the point model applications showed clearly that the surface energy balance was secondarily dominated by turbulent heat flux. This study, therefore, is in agreement with earlier investigations and can be added to a number of previous studies in mountainous areas that found net radiation fluxes and turbulent fluxes to account for approximately 70% and 30% of melt respectively (e.g. Marks and Dozier, 1992; Cline, 1997; Fox, 2003). Cumulative latent heat transfer during the modelled period was found to balance the positive sensible heat flux for the cases other than the rainfall and extreme weather conditions. Although high wind speeds were observed, especially at GY and CAT, periods of extremely cold weather conditions decreased the effect of turbulent heat fluxes; however, the ROS event observed in 2004 emphasized the effect of turbulent heat fluxes (sensible and latent heat), as reported elsewhere (e.g. Marks and Dozier, 1992; Cline, 1997; Marks *et al*., 1998; Anderton *et al*., 2002).

Model performance was tested against continuous records of SWE with snow pillows and change in snow depths measured with ultrasonic depth sensors, manual measurements of SWE and snow depths at snow courses, and water yield collected from snow lysimeters. The results were encouraging, because not only did simulated melt track measured runoff, but the model also showed how sensitive the melt process is to changes in climate conditions. The rate, amount and timing of snowmelt were accurately simulated according to SWE and snow depth measurements. The model was found to simulate rates of snow ablation effectively; there was very good agreement in the timing of observed and modelled SWE, except for the times of ice bridging.

Given the good agreement between observed and modelled SWE and snow depth, a possible explanation for the discrepancies with lysimeter outflow could be overflowing of the tipping bucket under the lysimeter and the non-uniform distribution of snow on the lysimeter and snow pillow. It had been anticipated that some improvements on the measurement of snowmelt yield from the lysimeter would be required.

Copyright © 2006 John Wiley & Sons, Ltd.

If the initial conditions and forcing data are reasonable representations of actual conditions, then SNOBAL can be used to estimate the timing, rate and amount of snowmelt generation accurately. The preparation of the forcing data for this work was very important; to improve some of the inputs, such as albedo, additional data will be needed in the future. It is acknowledged, however, that the spatial and temporal scales at which this work was carried out means that is unlikely to be of direct practical application in water resources management. The value of the results presented herein will be in the development of larger scale snowmelt models. Having tested SNOBAL output against observed data and found good agreement, model results can be used with some confidence in further investigations in Turkey related with snow models.

ACKNOWLEDGEMENTS

We would like to express our great appreciation to Dr Danny Marks for sharing his invaluable experience and comments. Thanks are also extended to the VIIIth Regional Directorate and General State Hydraulic Works of Turkey for their assistance before and during the site studies.

REFERENCES

Altınbilek D. 2004. Development and management of the Euphrates–Tigris basin. *International Journal of Water Resources Development* **20**(1): 15–33.

Anderson EA. 1976. *A point energy and mass balance model of a snow cover*. NOAA Technical Report NWS 19, US National Oceanic and Atmospheric Administration, Silver Spring, MD.

Anderton SP, White SM, Alvera B. 2002. Micro-scale spatial variability and the timing of snow melt runoff in a high mountain catchment. *Journal of Hydrology* **268**(1–4): 158–176.

Andreas EL. 1987. A theory for the scalar roughness and the scalar transfer coefficients over snow and sea ice. *Boundary Layer Meteorology* **38**: 159–184.

Cline DW. 1997. Snow surface energy exchanges and snowmelt at a continental, mid-latitude alpine site. *Water Resources Research* **33**(4): 689–701.

Cullen HM, Menocal PB. 2000. North Atlantic influence on Tigris–Euphrates streamflow. *International Journal of Climatology* **20**: 853–863.

Davis RE, Dozier J, Marks D. 1984. Micrometeorological measurements and instrumentation in support of remote sensing observations of an alpine snow cover. In *Proceedings of the 52nd Western Snow Conference*; 161–164.

Fox AM. 2003. *A distributed, physically based snowmelt and runoff model for alpine glaciers*. PhD dissertation, St Catherine's College, Oxford, UK.

Garen DC, Marks D. 2001. Spatial fields of meteorological input data including forest canopy corrections for an energy budget snow simulation model. In *Soil–Vegetation–Atmosphere Transfer Schemes and Large-Scale Hydrological Models*, Dolman H, Pomeroy J, Oki T, Hall A (eds). *IAHS Publication* No. 270. IAHS Press: Wallingford; 349–353.

Idso SB. 1981. A set of equations for full spectrum and 8- to 14 μm and 10·5- to 12·5 μm thermal radiation from cloudless skies. *Water Resources Research* **17**(2): 295–304.

Johnson JB, Marks D. 2004. The detection and correction of snow water equivalent pressure sensor errors. *Hydrological Processes* **18**: 3513–3525.

Kattelman R. 2000. Snowmelt lysimeters in the evaluation of snowmelt models. *Annals of Glaciology* **31**: 406–410.

Kaya HI. 1999. *Application of Snowmelt Runoff Model using remote sensing and geographic information systems*. MSc thesis, Department of Civil Engineering, Middle East Technical University, Ankara, Turkey.

Link TE, Marks D. 1998. Point simulation of seasonal snow cover dynamics beneath boreal forest canopies. *Journal of Geophysical Research* **104**(D22): 27 841–27 857.

Marks D. 1988. *Climate, energy exchange, and snowmelt in Emerald Lake watershed, Sierra Nevada*. PhD dissertation, Department of Geography and Mechanical Engineering, University of California: Santa Barbara, USA.

Marks D, Dozier J. 1992. Climate and energy exchange at the snow surface in the alpine region of the Sierra Nevada: 2. Snow cover energy balance. *Water Resources Research* **28**(11): 3043–3054.

Marks D, Winstral A. 2001. Comparison of snow deposition, the snow cover energy balance and snowmelt at two sites in a semiarid mountain basin. *Journal of Hydrometeorology* **2**(3): 213–227.

Marks D, Kimball J, Tingey D, Link T. 1998. The sensitivity of snowmelt processes to climate conditions and forest cover during rain on snow: a case study of the 1996 Pacific Northwest flood. *Hydrological Processes* **12**: 1569–1587.

Marks D, Domingo J, Frew J. 1999a. *Software tools for hydroclimatic modeling and analysis, Image Processing Workbench (IPW), ARS–USGS Version 2*. ARS Technical Bulletin 99-1, Northwest Watershed Research Center, Agricultural Research Service, Boise, Idaho, USA. http://www.nwrc.ars.usda.gov/ipw [22 June 2005].

Marks D, Domingo J, Susong D, Link T, Garen DC. 1999b. A spatially distributed energy balance snowmelt model for application in mountain basins. *Hydrological Processes* **13**: 1935–1959.

Marsh P. 1999. Snowcover formation and melt: recent advances and future prospects. *Hydrological Processes* **13**: 2117–2134.

Copyright © 2006 John Wiley & Sons, Ltd.

Moore RD. 1983. On the use of bulk aerodynamic formulae over melting snow. *Nordic Hydrology* **14**(4): 93–206.
Nash JE, Sutcliffe JV. 1970. River flow forecasting through conceptual models—Pt 1. *Journal of Hydrology* **10**(3): 282–290.
Satterlund DR. 1979. An improved equation for estimating longwave radiation from the atmosphere. *Water Resources Research* **15**(6): 1649–1650.
Şensory A. 2005. *Physically based point snowmelt modeling and its distribution in upper Karasu basin*. PhD dissertation, Department of Civil Engineering, Middle East Technical University, Ankara, Turkey.
Şensoy A, Tekeli AE, Şorman AA, Şorman AÜ. 2003. Simulation of event based snowmelt runoff hydrographs based on snow depletion curves and the degree day method. *Canadian Journal of Remote Sensing* **29**(6): 693–700.
Shusun L, Xiaobing Z, Morris K. 1999. Measurement of snow and sea ice surface temperature and emissivity in the Ross Sea. In *Proceedings of IEEE 1999 International Geoscience and Remote Sensing*.
Şorman AA. 2005. *Use of satellite observed seasonal snow cover in hydrological modeling and snowmelt runoff prediction in upper Euphrates basin, Turkey*. PhD dissertation, Department of Civil Engineering, Middle East Technical University, Ankara, Turkey.
Tekeli AE. 2005. *Operational hydrological forecasting of snowmelt runoff model by RS–GIS integration*. PhD dissertation, Department of Civil Engineering, Middle East Technical University, Ankara, Turkey.
Tekeli AE, Şorman AA, Şensoy A, Şorman AÜ, Bonta J, Schaefer G. 2005. Snowmelt lysimeters for real-time snowmelt studies in Turkey. *Turkish Journal of Engineering and Environmental Sciences* **29**(1): 29–40.

Copyright © 2006 John Wiley & Sons, Ltd.